Transcriptomic profiling of Polycystic Kidney Disease identifies paracrine factors in the early cyst microenvironment

Yasinoglu, S.A.; Kuipers, T.B.; Suidgeest, E.; Weerd, L. van der; Mei, H.L.; Baelde, H.J.; Peters, D.J.M.

BBA - Molecular Basis of Disease 1870 (2024) 166987

Contents lists available at ScienceDirect

BBA - Molecular Basis of Disease

journal homepage: www.elsevier.com/locate/bbadis

Transcriptomic profiling of Polycystic Kidney Disease identifies paracrine factors in the early cyst microenvironment

Sevtap A. Yasinoglu [a], Thomas B. Kuipers [b], Ernst Suidgeest [c], Louise van der Weerd [c], Hailiang Mei [b], Hans J. Baelde [d], Dorien J.M. Peters [a,*]

[a] Department of Human Genetics, Leiden University Medical Center, Leiden, the Netherlands
[b] Sequencing Analysis Support Core, Department of Biomedical Data Sciences, Leiden University Medical Center, Leiden, the Netherlands
[c] Department of Radiology, Leiden University Medical Center, Leiden, the Netherlands
[d] Department of Pathology, Leiden University Medical Center, Leiden, the Netherlands

ARTICLE INFO

Keywords:
Polycystic kidney disease
Cyst microenvironment
Cystic snowball effect
Laser capture microdissection
RNA sequencing

ABSTRACT

Initial cysts that are formed upon *Pkd1* loss in mice impose persistent stress on surrounding tissue and trigger a cystic snowball effect, in which local aberrant PKD-related signaling increases the likelihood of new cyst formation, ultimately leading to accelerated disease progression. Although many pathways have been associated with PKD progression, the knowledge of early changes near initial cysts is limited. To perform an unbiased analysis of transcriptomic alterations in the cyst microenvironment, microdomains were collected from kidney sections of iKsp-*Pkd1*^{del} mice with scattered *Pkd1*-deletion using Laser Capture Microdissection. These microdomains were defined as F4/80-low cystic, representing early alterations in the cyst microenvironment, F4/80-high cystic, with more advanced alterations, or non-cystic. RNA sequencing and differential gene expression analysis revealed 953 and 8088 dysregulated genes in the F4/80-low and F4/80-high cyst microenvironment, respectively, when compared to non-cystic microdomains. In the early cyst microenvironment, several injury-repair, growth, and tissue remodeling-related pathways were activated, accompanied by mild metabolic changes. In the more advanced F4/80-high microdomains, these pathways were potentiated and the metabolism was highly dysregulated. Upstream regulator analysis revealed a series of paracrine factors with increased activity in the early cyst microenvironment, including TNFSF12 and OSM. In line with the upstream regulator analysis, TWEAK and Oncostatin-M promoted cell proliferation and inflammatory gene expression in renal epithelial cells and fibroblasts in vitro. Collectively, our data provide an overview of molecular alterations that specifically occur in the cyst microenvironment and identify paracrine factors that may mediate early and advanced alterations in the cyst microenvironment.

1. Introduction

Autosomal dominant polycystic kidney disease (ADPKD) is a genetically heterogeneous disorder with an autosomal dominant pattern of inheritance, affecting 1 in 2500 individuals [1,2]. The main cause of disease is mutations in the genes *PKD1* (±78 %) and *PKD2* (±15 %), encoding the proteins polycystin-1 (PC1) and polycystin-2 (PC2), respectively [3–5]. Recent studies suggest that PC1 and PC2 can form a heterotetramer in a 1:3 ratio [6], while PC2 also can form homotetrameric channels [6–9]. Although the exact role of these proteins in tissue homeostasis and disease remains unclear, inadequate levels of polycystins have been shown to dysregulate cellular signaling and metabolism, ultimately leading to the formation of fluid-filled renal cysts [10–12]. These cysts initially arise from 1 to 5 % of the nephrons, and expand in number and size throughout life, resulting in end-stage renal disease by the age of 60 in 50 % of the patients [13,14]. Treatment with the vasopressin V2 receptor antagonist Tolvaptan has been shown to slow cyst growth and kidney function loss in patients, however, adverse effects of the drug (e.g. polyuria and hepatotoxicity) limit its wide application [15].

In the past decades, two models of cystogenesis have been proposed to drive initial cyst formation in ADPKD: the two-hit and the gene-dosage models [16–21]. These models describe that cyst formation may be triggered either by the loss of the wild-type *PKD1* or *PKD2* allele,

* Corresponding author at: Department of Human Genetics, Leiden University Medical Center, Leiden, the Netherlands.
E-mail address: d.j.m.peters@lumc.nl (D.J.M. Peters).

https://doi.org/10.1016/j.bbadis.2023.166987
Received 23 August 2023; Received in revised form 30 November 2023; Accepted 4 December 2023
Available online 8 December 2023

or by haploinsufficiency. However, it remains unclear which subsequent events lead to the progressive increase in the number of renal cysts in ADPKD patients. Our previous study in a slow-progressing mouse model for ADPKD has shown that, in the context of scattered *Pkd1*-gene disruption, cyst formation is accelerated upon formation of the initial cysts [22]. When disease progression was monitored over time, both an increase in cyst size and the number of new cysts were observed around initial cysts, resembling human ADPKD. In addition, several PKD-related molecular alterations were observed in the cyst microenvironment, both in cyst-lining epithelial cells and healthy-looking adjacent tubules. Based on these findings, we hypothesize that the initial cysts trigger a cystic snowball effect by induction of (mechanical) stress on the surrounding tissue, accompanied by hypoxia and injury-related mechanisms including the secretion of cytokines and growth factors, which subsequently alter signaling in the cyst microenvironment and give rise to additional cyst formation [22–24].

Previously, several studies have been conducted by us and others to profile PKD transcriptome using patient-derived material or whole kidneys from rats or mice to elucidate pathways associated with disease progression [25–27]. Although these studies provided valuable insights into PKD biology and pathology, a downside of bulk-RNA sequencing is that it represents average gene expression per kidney and the spatial information is lost. Therefore, changes that specifically occur in the cyst microenvironment may be masked and remain undetected. Also, the presence of immune infiltrates and their transcriptome in renal tissue could hinder the exploration of changes occurring in adjacent nephrons. In the present study, we addressed these issues through the use of Laser Capture Microdissection (LCM) to collect microdomains from the cyst microenvironment, preserving the spatial context. In addition, microdomain collection was guided by the expression of a monocyte/macrophage marker in the cyst microenvironment, as macrophages often accumulate in the vicinity of cysts and have been reported to contribute to epithelial cell proliferation and dedifferentiation, ultimately resulting in the progression of cystic kidney disease [28]. By focusing on the macrophage-low cyst microenvironment, we sought to find basal transcriptomic changes in epithelial cells and surrounding stroma near initial cysts that precede immune cell infiltration. Through the application of LCM in combination with ultra-low input RNA sequencing, we obtained a comprehensive overview of transcriptome alterations in the cyst microenvironment in iKsp-*Pkd1*^{del} mice and identified potential candidate paracrine factors that may drive altered signaling in the cyst microenvironment, ultimately leading to accelerated cyst formation and disease progression.

2. Methods

2.1. Mouse experiment

Tamoxifen-inducible kidney-specific *Pkd1* deletion mice (tam-Ksp-CreER^{T2};*Pkd1*$^{lox2\text{-}11;lox2\text{-}11}$) in short iKsp-*Pkd1*^{del} were generated on a full C57BL/6 genetic background as described before [29]. Scattered *Pkd1* deletion was induced via oral gavage of 12.5 mg/kg tamoxifen (T5648, Sigma Aldrich, dissolved in absolute ethanol) diluted in sunflower oil on PN18 and 19. Only male mice were included in the experiment since disease progression is slower in female mice [12,29]. Cyst formation was monitored monthly using MRI with a 7 T Bruker Pharmascan Biospin (Burker, Ettingen, Germany) as described previously, from PN105 until sacrifice [22]. Blood urea (BU) levels were measured using the Reflotron® Sprint (Roche Diagnostics, Mannheim, Germany) at PN139-141 and before sacrifice. After sacrifice, kidneys were taken out and weighed for calculation of the 2 kidney weight to body weight (2KW/BW) ratio. Following, bisected kidneys were either snap-frozen in isopentane pre-chilled with dry ice or fixed in 4 % buffered formaldehyde. Snap-frozen kidneys were stored at −80 °C until further use. All the animal experiments were approved by the Animal Experiment Ethics Committee of Leiden University Medical Center and the Commission of Biotechnology in Animals of the Dutch Ministry of Agriculture (AVD1160020197684), and performed in accordance to Directive 2010/63/ EU for animal experiments.

2.2. Immunohistochemistry

Fresh kidneys, fixed overnight in 4 % buffered formaldehyde, were embedded in paraffin and sectioned at 4 μm thickness. Sections were subjected to antigen retrieval (Suppl. Table 1), blocked with 0.1 % H_2O_2 for 20 min to inhibit endogenous peroxidase activity, and pre-incubated with 5 % normal goat serum in 1 % BSA in PBS for 1 h. Next, the sections were incubated with the primary and secondary antibodies listed in Supplementary Table 1. Immune reactions were revealed using diaminobenzidine as a chromogen (ab64238). Following, the sections were counterstained with Mayer's hematoxylin for 10 s, dehydrated, and mounted.

2.3. Laser capture microdissection (LCM)

PEN membrane glass slides (Carl Zeiss™ Membrane Slides; 415190-9041-000) were irradiated with UV light for 30 min before use. Snap-frozen kidneys were sectioned sequentially at 10 μm thickness, mounted onto room temperature PEN membrane glass slides, and immediately stored in 50 ml Falcon tubes at −80 °C until microdissection. Stored sections were allowed to equilibrate to room temperature before microdissection, rehydrated, and stained with Mayer's hematoxylin in the following order: 70 % ethanol 30 s, dip in water 10 times, hematoxylin 10 s, dip in water 10 times, dip in water 10 times, 70 % ethanol 1 min, 90 % ethanol 1 min, 100 % ethanol 1 min, 100 % ethanol 1 min, air dry, xylene 1 min, xylene 1 min, and air dry. Microdissection was performed using Zeiss PALM Microbeam Laser Microdissection Microscope and the catapulted tissue was captured into adhesive caps (Carl Zeiss™ Adhesive Caps; 10138374). Collected samples were placed on dry ice until TRI Reagent® (Sigma-Aldrich) was added. RNase-free conditions were ensured during all steps of the experiment.

To guide microdissection, snap-frozen kidneys were sectioned (sequential to the tissue collection sections of 10 μm thick) at 4 μm thickness and air-dried. The sections were fixed with 1 % neutral buffered formalin for 20 min and blocked with 5 % normal goat serum in 1 % BSA for 30 min. Subsequently, slides were incubated with anti-F4/80 antibody, followed by Anti-rat Immpress HRP. Based on this staining, the following microdomains were collected from PKD kidney sections: F4/80-low non-cystic (LNC), F4/80-low cystic (LC), and F4/80-high cystic (HC). Collected microdomains were from the cortex in all experiments.

For qPCR analysis experiments, 3 sequential sections (10 μm thick) were used for tissue collection and the selected microdomains from these 3 sections were pooled (±100.000 μm^2 tissue in total after pooling). For the RNA-sequencing experiment, 6 sequential sections (10 μm thick) were used for tissue collection (±300.000 μm^2 in total after pooling). To ensure that all pooled microdomains were from either F4/80-low or F4/80-high regions, 2 adjacent sections (4 μm thick, 1 section before and 1 section after the 6 sections used for microdissection) were used for the F4/80 IHC staining. For RNA sequencing, 2 microdomains were collected per group (LNC, LC, or HC) per mice (age 269 and 297), from 3 different male mice (n = 6 per group). An overview of the experimental set-up is shown in Supplementary Fig. 1.

2.4. RNA isolation and quantitative PCR

Microdissected regions captured in adhesive caps were incubated upside down for 15 min with 300 μl TRI Reagent® (Sigma-Aldrich) supplemented with 5 μl β-Mercaptoethanol (Sigma-Aldrich) and transferred to a fresh 1.5 ml tube. To isolate total RNA, 60 μl chloroform was added per 300 μl TRI Reagent® and the aqueous phase was transferred to a fresh tube. RNA was precipitated using 150 μl isopropanol and 5 μl 20 mg/ml glycogen (Roche Life Science). RNA pellets were dissolved in 5.5 μl water and reverse transcribed to cDNA with the Transcriptor First Strand cDNA Synthesis Kit (Roche Life Science) according to the

manufacturer's instructions. cDNA was diluted (1:12.5) and qPCR was performed using the FastStart Universal SYBR Green Master (Rox) (Sigma-Aldrich), according to the manufacturer's protocol.

Before qPCR experiments, we evaluated the suitability of commonly used housekeeping genes as a reference control for our qPCR normalization, since inflammation could modulate housekeeping gene expression in tissues [30–32]. Among the evaluated housekeeping genes (*Hprt*, *Rpl13a*, *Actb*, *18s rRNA*, and *Gapdh*) *Actb* and *Gapdh* appeared to be least stable, as increased *Actb* and decreased *Gapdh* mRNA levels were found in HC microdomains (Supplementary Fig. 2A). In contrast, *Hprt* and *Rpl13a* showed stable expression across collected microdomains and correlated well (Pearson $r = 0.94$) (Suppl. Fig. 2A–C). Accordingly, *Hprt* and *Rpl13a* were used to normalize qPCR data using the ΔΔCT method. The primer sequences are listed in Supplementary Table 2.

2.5. RNA quality assessment

Quality and reliability of mRNA (obtained from microdomains) were evaluated, by testing different RNA isolation protocols: cell lysis only [33], Nucleospin RNA XS micro kit (according to the manufacturer's instructions), RNeasy micro kit (according to the manufacturer's instructions), and TRI reagent (as described above). Accordingly, cDNA fragment length was assessed following an oligo(dT)-primed cDNA synthesis and cDNA amplification step, and cDNA was loaded on a High sensitivity DNA LabChip (Suppl. Fig. 3A and 3B). Briefly, lysis of the tissue using only lysis buffer (0.2 % Triton X-100 and 2 U/μl of RNase inhibitor) was not sufficient to yield enough cDNA. cDNA of comparable fragment size were obtained using RNA isolation kits and the TRI reagent. Since RNA isolation using TRI reagent followed by oligo(dT)-primed cDNA synthesis yielded good quality (>1 kb fragment length) and high concentration cDNA, our RNA isolation protocol was not further adjusted.

2.6. Ultra-low input RNA sequencing

Sequencing libraries were prepared from 4 μl total RNA (<250 picograms) per microdomain using the NEBNext® Single Cell/Low Input RNA Library Prep Kit from Illumina® (E6420) according to the manufacturer's instructions by GenomeScan (Leiden, The Netherlands). Briefly, Unique molecular identifiers (UMIs) were included to ensure the identification of PCR artifacts. cDNA was PCR amplified for 21 cycles and the libraries were PCR amplified for 8 cycles. AMPure XP beads were used for the clean-up steps. High sensitivity NGS Fragment analysis kit (Agilent) was used to assess library quality and all samples passed the quality control. The average library fragment size was 550 bp. The samples were sequenced by GenomeScan (Leiden, The Netherlands) with 30 M read depth per sample on Illumina NovaSeq 6000 to obtain 150 bp paired-end reads.

2.7. RNA sequencing data processing

RNA sequencing raw data processing was performed by GenomeScan (Leiden, The Netherlands). Sequence reads were trimmed to remove possible adapter sequences using fastp v0.20.1. For each sample, trimmed reads were mapped to the mouse genome mm10 2020-A using STAR2 v2.5.4. Gene count tables were generated using HTSeq v0.11.0 with gene annotation Ensembl GRCm38 (version m23), release 98.

2.8. Differential gene expression analysis

Differential gene expression analysis was performed for the comparisons between F4/80-low or F4/80-high cystic microdomains and F4/80-low non-cystic microdomains using DESeq2 v1.14.1. Genes were considered as differentially expressed if the adjusted *p*-value was <0.05. Volcano plots were generated in GraphPad Prism 8 (GraphPad Software, La Jolla California USA).

2.9. Gene set enrichment analysis

Gene set enrichment analysis was used to infer the functions of the genes by ranking all measured genes on fold change expression, without the application of a p-value threshold. All measured genes were included in the analysis with a BaseMean >20. Subsequently, enriched Gene Ontology terms (biological processes (BP), cellular components (CC), and molecular functions (MF)) were determined using clusterProfiler package v4.2.0, org.Mm.eg.db package v3.14.0, and gseGO() function using default settings.

2.10. Pathway analysis

The canonical pathway analysis was generated through the use of Ingenuity Pathway Analysis (IPA) software (Qiagen). Only differentially expressed genes (DEGs) (adjusted *p*-value <0.05) were included in the analysis, while the complete gene list was used as a reference set. Canonical pathways with an adjusted p-value <0.05 were considered significant. In addition to pathway analysis, the activity of canonical pathways was predicted using z-score statistics [34]. Z-scores of <−2 and >2 were taken as the threshold for significant inhibition and activation, respectively.

2.11. Upstream regulator analysis

Upstream regulator analysis was performed using IPA software (Qiagen). In this analysis, IPA identifies upstream regulators based on expected causal effects between upstream molecules and target genes, and predicts the activity of the protein encoded by the upstream regulator gene [34]. Bias-corrected z-scores of <−2 and >2 were taken as the threshold for significant inhibition and activation, respectively. Bias-corrected z-scores were shown in Tables 1 and 2, which account for the dataset bias when more up-than-down-regulated genes are present in the dataset.

2.12. Microenvironment cell population counter analysis

To estimate the tissue infiltrating immune cell and stromal cell composition in different microdomains, mMCP counter R package v1.1.0 was used as described previously [35]. Briefly, log2(1 + TPM) count matrix was used as input for the analysis. Based on pre-defined distinct cell populations and their specific gene expression signature, cell populations in the microdomains were scored to examine their abundance in the microdomains. The scores are proportional to the amount of estimated cell populations in the sample and are expressed in arbitrary units. These scores allow comparison of the abundance of one cell population between samples.

2.13. Cell culture

Pkd1^{wt} and *Pkd1*$^{-/-}$ murine proximal tubular epithelial cells (mPTECs) were derived from a *Pkd1* ^{lox,lox} mouse and immortalized using SV40 large T antigen. *Pkd1*$^{-/-}$ cells were obtained from *Pkd1*^{lox,lox} cells upon transfection with a Cre plasmid as described before [36]. Human renal fibroblast cell line TK173 (derived from a healthy human kidney) was a kind gift provided by Prof. Gerhard A. Müller, Department of Nephrology and Rheumatology, Georg August University, Göttingen, Germany [37]. Cells were maintained at 37 °C and 5 % CO2 in DMEM/F-12 with GlutaMAX (Gibco, Life Technologies; 31331-093) supplemented with 100 U/ml Penicillin–Streptomycin (Gibco, Life Technologies; 15140-122) and 9 % Fetal Bovine Serum (Biowest; S1810). RNA and cDNA from cultured cells were obtained using TRI Reagent® (Sigma-Aldrich) and the Transcriptor First Strand cDNA Synthesis Kit (Roche Life Science) according to the manufacturer's instructions.

Table 1
Cytokines with increased activity in F4/80-low cystic microdomains vs F4/80-low non-cystic microdomains. Upstream regulator analysis (URA) was performed in IPA software and the cytokines with predicted increased activity (z-score >2) were shown and ordered by the highest bias-corrected z-score (left panel). Fold change expression of the cytokines and cytokine receptors were also presented (middle and right panel: differential gene expression analysis (DGEA)). For the complete list of the URA including downstream target genes, see Suppl. Table 7.

Cytokine	URA		DGEA LC vs LNC		Receptor	DGEA LC vs LNC	
	Bias-corrected z-score	B-H corrected p-value	Fold change	Adjusted p-value		Fold change	Adjusted p-value
IFNG	6,08	3,04E-51	1,17	1,00E+00	IFNGR1	1,57	2,43E-03
					IFNGR2	2,17	1,85E-06
TNF	5,51	9,45E-50	1,19	1,00E+00	TNFRSF1A	1,90	1,81E-03
					TNFRSF1B	1,99	6,69E-02
IL1B	5,48	1,19E-29	1,52	3,54E-01	IL1R1	1,23	7,00E-01
					IL1RAP	0,81	6,14E-01
OSM	4,35	9,42E-16	1,03	1,00E+00	OSMR	1,90	8,99E-03
IL6	3,95	3,90E-35	1,09	1,00E+00	IL6RA	1,43	4,41E-01
IL1A	3,70	8,85E-18	0,69	4,71E-01	IL1R1	1,23	7,00E-01
					IL1RAP	0,81	6,14E-01
CNTF	3,47	2,69E-09	1,54	3,67E-01	CNTFR	0,60	2,67E-01
IL2	3,46	3,17E-18	1,19	1,00E+00	IL2RA	1,05	1,00E+00
					IL2RB	1,23	7,56E-01
TNFSF12	3,43	9,13E-11	1,48	8,85E-02	TNFRSF12A	2,22	6,12E-03
IL27	2,96	2,46E-14	0,97	1,00E+00	IL27RA	1,92	9,95E-02
CSF1	2,89	9,12E-21	2,20	4,43E-03	CSF1R	1,67	1,18E-04
IL33	2,80	2,70E-26	1,82	1,46E-02	IL1RL1	1,83	1,55E-01
PRL	2,78	7,36E-18	1,03	1,00E+00	PRLR	1,68	1,00E+00
TNFSF11	2,60	8,93E-17	1,01	1,00E+00	TNFRSF11B	1,25	1,00E+00
TNFSF13B	2,45	1,27E-07	2,23	6,36E-03	TNFRSF13B	1,19	8,17E-01
C5	2,42	8,05E-10	1,05	1,00E+00	C5AR1	2,52	7,62E-03
EBI3	2,29	1,14E-07	1,20	7,93E-01	IL27RA	1,92	9,95E-02
CSF2	2,27	1,38E-30	1,04	1,00E+00	CSF2RA	2,08	2,70E-03
CXCL12	2,22	5,78E-12	1,19	6,34E-01	CXCR4	1,67	1,00E+00
IL18	2,19	1,14E-09	1,05	9,28E-01	IL18R1	1,12	8,83E-01
CD40LG	2,15	1,33E-13	1,05	1,00E+00	CD40	2,33	8,04E-03
IL12A	2,10	2,42E-04	1,03	1,00E+00	IL12RB1	1,13	1,00E+00

Table 2
Growth factors with increased activity in F4/80-low cystic microdomains vs F4/80-low non-cystic microdomains. Upstream regulator analysis (URA) was performed in IPA software and the growth factors with predicted increased activity (z-score >2) were shown and ordered by the highest bias-corrected z-score (left panel). Fold change expression of the growth factors and growth factor receptors were also presented (middle and right panel: differential gene expression analysis (DGEA)). For the complete list of the URA including downstream target genes, see Suppl. Table 7.

Growth factor	URA		DGEA LC vs LNC		Receptor	DGEA LC vs LNC	
	Bias-corrected z-score	B-H corrected p-value	Fold change	Adjusted p-value		Fold change	Adjusted p-value
TGFB1	6,11	2,01E-52	1,30	6,63E-01	TGFBR1	1,10	7,92E-01
					TGFBR2	1,86	1,11E-06
					TGFBR3	1,24	5,60E-01
AGT	5,7	1,24E-43	3,27	6,14E-05	AGTR1A	0,97	9,52E-01
PDGFB	2,37	1,55E-05	2,06	1,83E-04	PDGFRB	2,24	5,17E-07
FGF8	2,30	8,20E-03	0,96	1,00E+00	FGFR1	1,31	2,29E-01
NRG1	2,25	5,33E-04	1,40	2,77E-01	ERBB3	1,05	9,10E-01
					ERBB4	1,66	1,75E-01
AREG	2,19	3,02E-03	1,40	1,00E+00	EGFR	1,07	8,28E-01
FGF2	2,13	1,40E-20	0,84	6,74E-01	FGFR1	1,31	2,29E-01
FGF7	2,06	4,09E-03	1,11	1,00E+00	FGFR2	0,92	9,21E-01
EGF	2,06	1,26E-11	0,81	7,03E-01	EGFR	1,07	8,28E-01

2.14. PrestoBlue cell viability assay

PrestoBlue cell viability reagent (Invitrogen, A13261) was used to quantitatively measure the proliferation of cells, according to the manufacturer's instructions. On day 1, *Pkd1*^{wt} mPTEC, *Pkd1*$^{-/-}$ mPTEC, and TK173 cells were seeded in a 96-well plate and allowed to attach and acclimate for 24 h. On day 2, cells were washed with PBS and serum starved overnight. On day 3, 60–70 % confluent cells were stimulated with either recombinant human TWEAK (Peprotech; 310-06) or recombinant human Oncostatin M (Peprotech; 300-10H) at 100 ng/ml concentration for 24 h. 5 wells were stimulated per group per independent experiment. On day 4, cells were incubated in 10 % PrestoBlue reagent in serum free medium for 2 h. Following, the fluorescence was measured using a multi-mode microplate reader (iD3-4109) with excitation and emission wavelengths 555 nm and 595 nm, respectively.

2.15. Statistical analysis

Statistical analyses were performed with GraphPad Prism 8 (GraphPad Software, La Jolla California USA) or R packages. All qPCR results were expressed as mean ± SD. Comparisons between 2 groups were done using the two-tailed unpaired Student's *t*-test and the comparisons between more groups were done using one-way ANOVA, followed by either Tukey's or Dunn's multiple comparisons tests. Right-tailed Fisher's Exact test was used to calculate the significance of the canonical pathways and the Benjamini-Hochberg corrected *p*-values <0.05 were considered significant.

3. Results

3.1. The cystic snowball mouse model

Pkd1 inactivation at PN18 using standard dose (150 mg/kg) tamoxifen typically leads to the formation of cysts in the cortex and outer medulla, which are more equally distributed over different nephron segments compared to the PN40 model [22,23]. To generate mice with scattered *Pkd1* deletion, we treated iKsp-*Pkd1*^{del} mice (PN18-19) with a low dose (12.5 mg/kg) of tamoxifen to induce Cre activation in a low percentage of cells, essentially as done before for the PN40 model [22]. Accordingly, PKD progression was followed by MRI to allow sacrificing at a mild cystic phase of the disease (Fig. 1A, B, and E). This phase was reached between 8 and 9 months after tamoxifen as observed by MRI and histology. In these mice, the 2KW/BW ratio was increased when compared to the age-matched control mice (Fig. 1C). In line with this, blood urea (BU) levels at sacrifice were also increased when compared to BU levels at 4 months after tamoxifen. Only 3 mice reached the onset of end-stage renal disease (BU >20 mmol/L) (Fig. 1D). Overall, the majority of mice had mild to moderate cystic disease with multiple cyst clusters formed predominantly in the cortex and outer medulla.

3.2. Isolation of different microdomains from the cyst microenvironment using laser capture microdissection (LCM)

To analyze alterations in the cyst microenvironment we first defined microdomains to discriminate early alterations (before inflammation) from more advanced alterations (during inflammation) based on the protein expression of kidney injury marker LCN2 and murine monocyte/macrophage marker F4/80. These markers are frequently co-expressed in the cystic microenvironment, suggesting that monocytes/macrophages accumulate around injured tubules (Fig. 2A). In addition, we show that the broad myeloid marker CD11b was also enriched in F4/80-high regions around cysts, while the expression was lower in F4/80-low regions (Suppl. Fig. 4). Next, we used laser capture microdissection (LCM) to collect microdomains based on F4/80 protein expression in tissue near cysts, distant non-cystic regions and wild type kidneys. Subsequently, mRNA expression of F4/80 (*Adgre1*) and alternative myeloid/lymphoid cell marker genes *Mrc1* and *Cd74* were validated (Fig. 2B and D). As expected, gene expression levels of these markers were increased in cystic microdomains with high F4/80 protein expression (F4/80-high cystic (HC)) when compared with F4/80-low cystic (LC), F4/80-low non-cystic (LNC), and wild-type (WT) microdomains, where the F4/80 positive cells were scarce. Similarly, *Lcn2* mRNA expression was highly increased in HC microdomains when compared with LC, LNC, and WT microdomains (Fig. 2C). Accordingly, F4/80 was selected as a guidance marker for microdomain selection, since F4/80 gene expression was consistent with the observed protein expression, the gene expression was less variable between isolated microdomains, and the anti-F4/80 antibody performance was optimal on frozen tissue sections.

3.3. Microdomain-specific alterations in gene expression in the cyst microenvironment

To explore further whether there is a difference in signaling in the different microdomains, we analyzed gene expression of the pregnancy-associated plasma protein A (PAPP-A) and insulin-like growth factor 1 (IGF-1) signaling pathway members. Recently, PAPP-A/IGF-1 signaling has been suggested to play a key role in the regulation of cyst growth and expansion [38]. We found increased *Igf1* expression in cystic regions with high *Adgre1* expression, while the expression of *Pappa*, *Igfbp4*, *Igfbp5*, *Igf1r*, *Irs1*, and *Irs2* were significantly decreased compared to the WT and LNC microdomains (Fig. 2E). None of these genes were significantly altered in LC microdomains when compared to WT and LNC microdomains. These findings suggest altered IGF-1 signaling particularly in regions with high monocyte/macrophage infiltration. However, because of the complexity of the IGF-1R signaling, it is difficult to draw

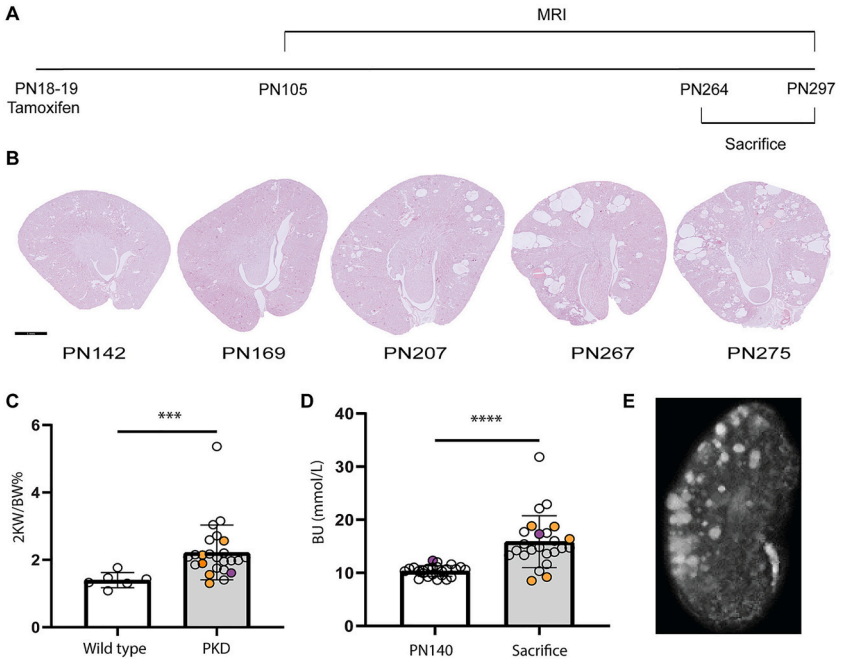

Fig. 1. Generation of cystic snowball mice. **(A)** Timeline of mice treated with tamoxifen at PN18 and 19. Mice were followed by MRI analysis in time from PN105 until sacrifice. A total of 4 animals were sacrificed between PN142 and 207 to confirm cystic phenotype and remaining animals ($n = 20$) were sacrificed between PN264 and 297. **(B)** Representative images of PAS-stained kidney sections of mice at the indicated time points. Scale bar; 1 mm. **(C)** 2KW/BW% at sacrifice. **(D)** Blood urea (BU) levels at PN140 (pre-cystic phase) and sacrifice. **(C** and **D)** Each data point represents a single mouse. Orange-filled data points represent mice shown in panel B and purple-filled data points represent the mouse shown in panel E. Data represent the mean ± SD. Significance was measured by Student's *t*-test. * *P* value <0.05; ** P value <0.01; *** P value 0.001; **** P value 0.0001. **(E)** 2D reconstruction of a mild mouse kidney imaged at PN274. PN: postnatal, MRI: Magnetic Resonance Imaging.

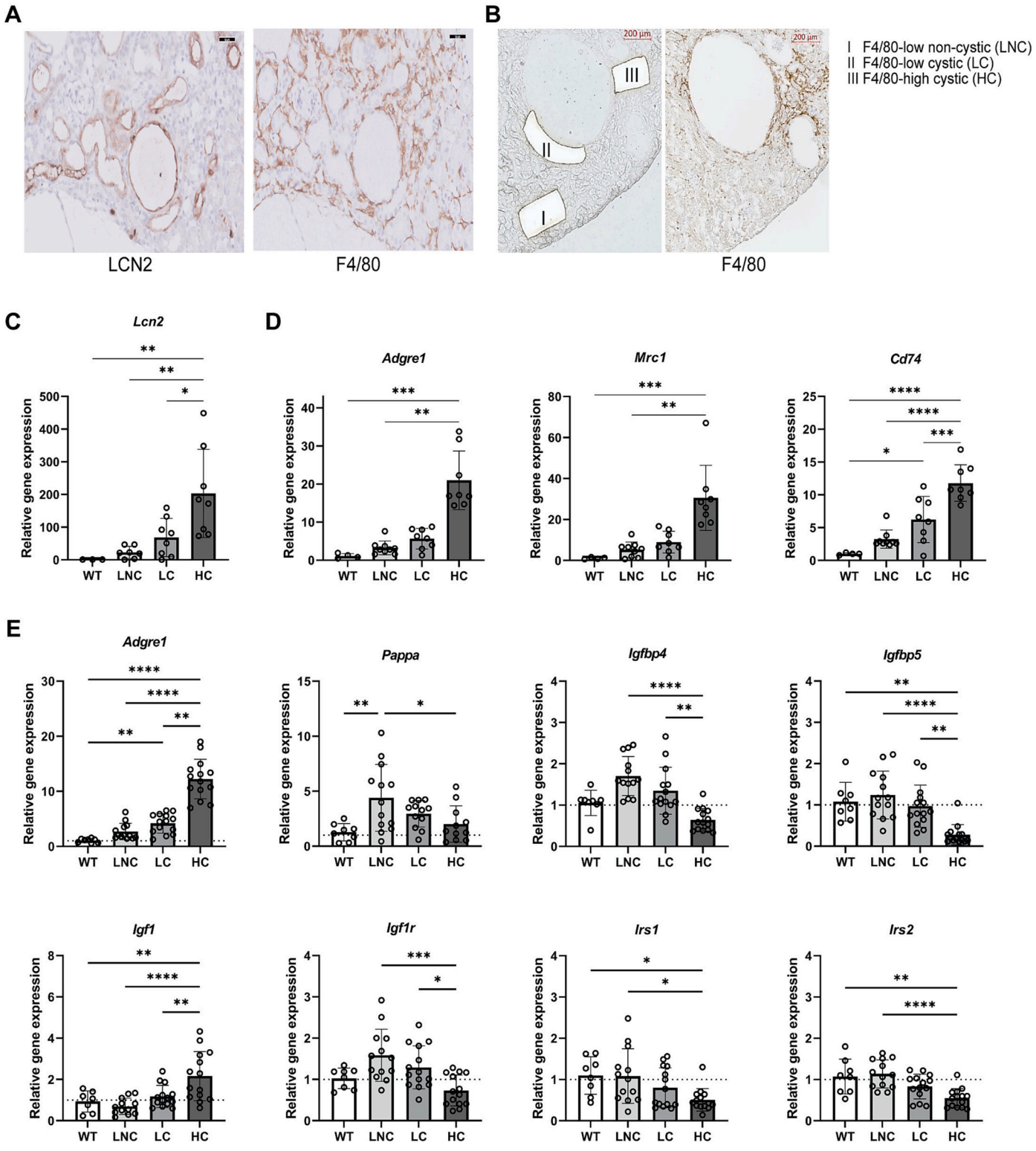

Fig. 2. Classification of microdomains within the cyst microenvironment and PAPP-A/IGF signaling in different microdomains. **(A)** Serial paraffin sections were stained for LCN2 (kidney injury marker) and F4/80 (monocyte/macrophage marker). Scale bar: 50 µm. **(B)** Representative image of regions isolated by Laser Capture Microdissection from frozen kidney section (left) with F4/80 staining of the adjacent kidney section (right). I: F4/80-low non-cystic (LNC), II: F4/80-low cystic (LC), and III: F4/80-high cystic (HC). Scale bar: 200 µm. **(C)** Gene expression of *Lcn2* in LNC, LC, and HC microdomains collected from cystic kidneys and compared with microdissected regions from age-matched wild type (WT) control kidneys. **(D)** Gene expression of selected myeloid/lymphoid markers *Adgre1*, *Mrc1*, and *Cd74* in LNC, LC, and HC regions collected from cystic kidneys compared to microdissected regions from age-matched WT control kidneys. **(C** and **D)** Each data point represents a single microdissected region collected from 2 mice. Data represent the mean ± SD. Significance was measured by one-way ANOVA. **(E)** Gene expression of *Adgre1*, *Pappa*, *Igfbp4*, *Igfbp5*, *Igf1*, *Igf1r*, *Irs1*, and *Irs2* in collected microdomains from PKD kidneys when compared to the expression in microdomains from WT kidneys. Each data point represents a single microdissected region collected from 3 mice. Data represent the mean ± SD. Significance was measured by one-way ANOVA. * *P* value <0.05; ** P value <0.01; *** P value 0.001; **** P value 0.0001.

firm conclusions from these data [39].

3.4. RNA sequencing analysis of the cyst microenvironment

To acquire a comprehensive and unbiased profile of dysregulated gene expression in the cyst microenvironment, we performed ultra-low input RNA sequencing. We found 953 and 8088 genes differentially expressed in LC and HC microdomains, respectively, when compared to the non-cystic regions. In addition, 5929 genes were altered when HC microdomains were compared to LC microdomains (Fig. 3A and Suppl. Table 3). Among the 899 differentially expressed genes (DEGs) that were shared between LC vs LNC and HC vs LNC comparisons, 621 genes were also in overlap with the HC vs LC comparison, while only 278 genes were shared between LC vs LNC and HC vs LNC (Fig. 3B and Suppl. Table 4). In addition, in both LC and HC microdomains (compared to LNC), more genes were upregulated than downregulated, while the genes were more significantly dysregulated in HC microdomains (Fig. 3C and Suppl. Table 3). In line with this, the heatmap of the top 500 differentially expressed genes (LC vs LNC) shows altered gene expression in LC microdomains compared to LNC, while these genes were more strongly dysregulated in HC microdomains (Fig. 3D). Together, these data indicate that gene expression profiles of the cyst microenvironment are highly altered compared to non-cystic regions. In addition, alterations that already occur before macrophage accumulation appear to be stronger in macrophage-dense regions, and accompanied by more dysregulated genes. However, identified differentially expressed genes in HC microdomains can also be attributed to the immune cells that are present in the cyst microenvironment, rather than being solely epithelial cell and stroma-specific alterations.

To get a better understanding in the immune cell composition in LNC, LC, and HC microdomains, we performed cell type deconvolution using murine Microenvironment Cell Population counter (mMCP-counter) [35]. Using a set of signatures genes, mMCP-counter estimated the relative abundance of tissue-infiltrating immune cell and stromal cell populations in each sample, allowing comparison of specific immune cell abundance between different microdomains (Suppl. Fig. 5A and B). In addition to macrophages, we also found T cell and fibroblast enrichment in HC microdomains compared to LC and LNC microdomains (Suppl. Fig. 5A). Immunohistochemical staining for T cell and myofibroblast markers showed that CD3-positive T cells were often present at much lower numbers in the cyst microenvironment compared to macrophages, while α-smooth muscle actin-positive myofibroblasts were highly enriched in macrophage-dense cyst microenvironment (Suppl. Fig. 6). These findings confirm that LC microdomains were low in macrophages and other immune cells, suggesting that transcriptomic alterations found in LC microdomains can largely be attributed to the cyst surrounding epithelial cells and stroma. Therefore, it is likely that alterations found in these regions are the earlier, initial alterations in the cyst microenvironment.

3.5. Enriched biological functions in the cyst microenvironment

To get insight into the biological processes altered in the cyst microenvironment, Gene Set Enrichment Analysis (GSEA) was performed. Top 25 most significantly enriched GO terms in LC microdomains were related to extra cellular matrix, angiogenesis, cell adhesion, cell migration, tube morphogenesis and immune responses (Fig. 4A and Suppl. Table 5 (complete list)). In HC microdomains, mitochondrial protein complex, mitochondrial matrix, and a variety of catabolic and metabolic processes were highly enriched in addition to extra cellular matrix and immune response related processes (Fig. 4B and Suppl. Table 5). Overall, these data indicate that tissue remodeling, immune response and metabolism-related processes were enriched in the cyst microenvironment, where LC microdomains were characterized by tissue remodeling-related processes, while metabolism and inflammation-related processes were more pronounced in HC microdomains.

3.6. Dysregulated canonical pathways in the cyst microenvironment

Ingenuity Pathways Analysis (IPA) was used to confirm GSEA and to examine canonical pathways associated with the DEGs in the cyst microenvironment.

3.6.1. Early alterations in F4/80-low cyst microenvironment

Similar to the enriched GO terms, most prominent activated canonical pathways in LC microdomains (compared to LNC) were largely linked to tissue remodeling (e.g. Fibrosis, Wound Healing, GP6, Rho Family GTPases, Integrin, and Actin Cytoskeleton Signaling), initiation of immune responses (e.g. Phagosome Formation, Dendritic Cell Maturation, Acute Phase Response, Interleukin Signaling, and Chemokine Signaling), hypoxia (e.g. HIF1α signaling), and cellular growth and proliferation (e.g. ERK/MAPK signaling) (Fig. 5 and Suppl. Table 6 (complete IPA list)). Mechanical stress-related pathways were also activated, including Integrin Signaling, Signaling by Rho Family GTPases, Actin cytoskeleton signaling, and RAC signaling [40,41]. Elevated activity of these pathways suggests that injury-repair processes were already activated in LC microdomains [25]. Only limited number of pathways were suppressed, including Oxidative Phosphorylation, PTEN, RHOGDI, and PPAR signaling (Fig. 5 and Suppl. Table 6). Together, these results suggest that several injury-related processes and mild metabolic alterations occur in the cyst microenvironment, even when the tissue surrounding cysts appears normal and lacks massive macrophage infiltration.

3.6.2. More advanced alterations in F4/80-high cyst microenvironment

Most of the canonical pathways that were activated or inhibited in LC microdomains were more strongly dysregulated in HC microdomains (compared to LNC) as indicated by higher (absolute) z-scores (Fig. 5A and Suppl. Table 6). However, pathways involved in innate immunity (e.g. Phagosome Formation, Dendritic Cell Maturation, IL-15 Production, MIF Regulation of Innate Immunity, and Coagulation system) were more significantly dysregulated in LC microdomains. Furthermore, we identified a substantial number of pathways that were only significantly dysregulated in HC microdomains (Fig. 5B). Among these, p70S6K (mTORC1 effector), P2Y Purinergic receptor signaling, PI3K/AKT, CXCR4, TGF-β, Renin-Angiotensin, HGF, STAT3, JAK/STAT, TNFR, and IGF-1 signaling have been associated with ADPKD progression previously, based on in vitro experiments, analysis of whole kidney lysates, and/or mouse studies (Fig. 5B) [38,42–50]. Activated IGF signaling particularly in HC microdomains confirms and complements our qPCR data (Fig. 2E). However, several other pathways related to PKD progression, such as cAMP signaling or programmed cell death (e.g. apoptosis and ferroptosis) were either not significantly dysregulated or not significantly activated according to IPA, although a subset of genes show differential expression (Suppl. Table 6). Furthermore, several signaling pathways previously linked to cancer were activated in these regions (e.g. PAK, Telomerase, FAT10 Cancer Signaling) [49,51–53]. Importantly, a considerable number of metabolic processes showed reduced activation, including multiple metabolite breakdown and biosynthesis pathways, Ketogenesis, Fatty Acid β-oxidation, and TCA cycle (Fig. 5B).

Pathways with significantly dysregulated activity in HC microdomains compared to LC were mainly associated with tissue remodeling (e.g. Fibrosis, Wound Healing, GP6, Rho Family GTPases, and Integrin Signaling), Acute Phase Response Signaling, and inflammatory responses (e.g. Leukocyte Extravasation, Crosstalk Between Dendritic Cells and Natural Killer Cells, Fcγ Receptor-mediated Phagocytosis in Macrophages and Monocytes, and PI3K signaling in B Lymphocytes) (Suppl. Fig. 7 and Suppl. Table 6). Similar to the HC vs LNC comparison, several metabolic processes were suppressed, with some additional metabolic pathways uniquely dysregulated in HC vs LC comparison,

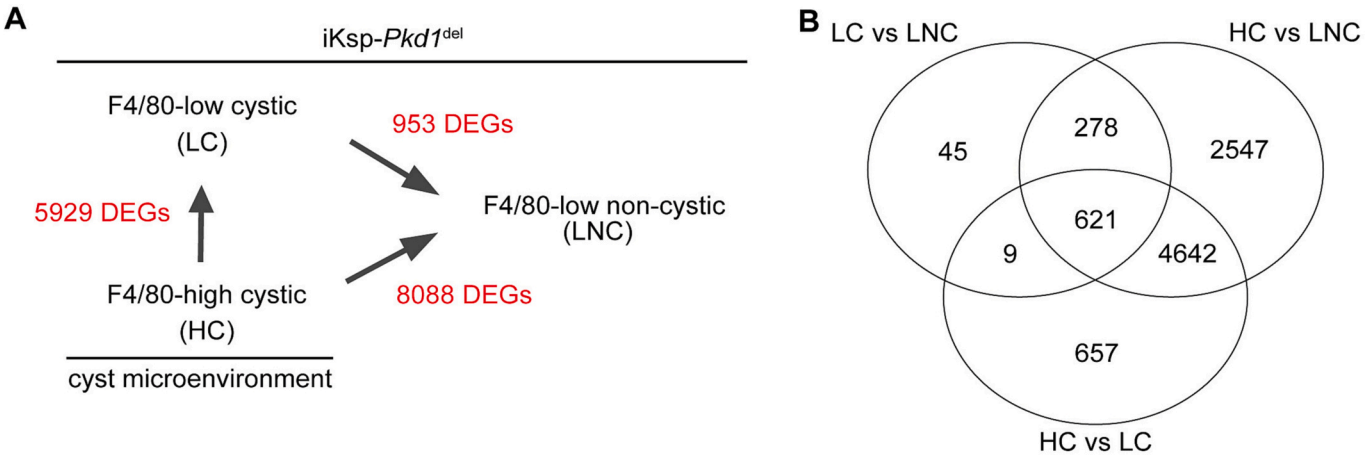

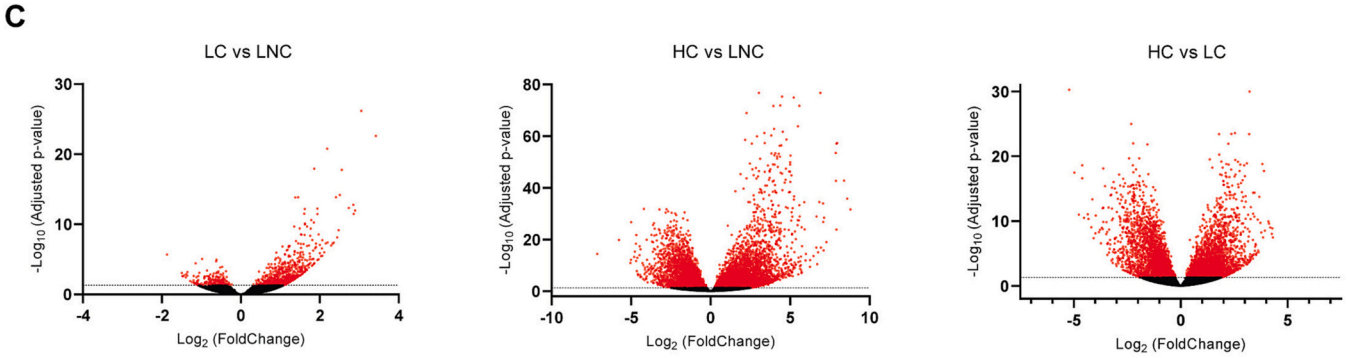

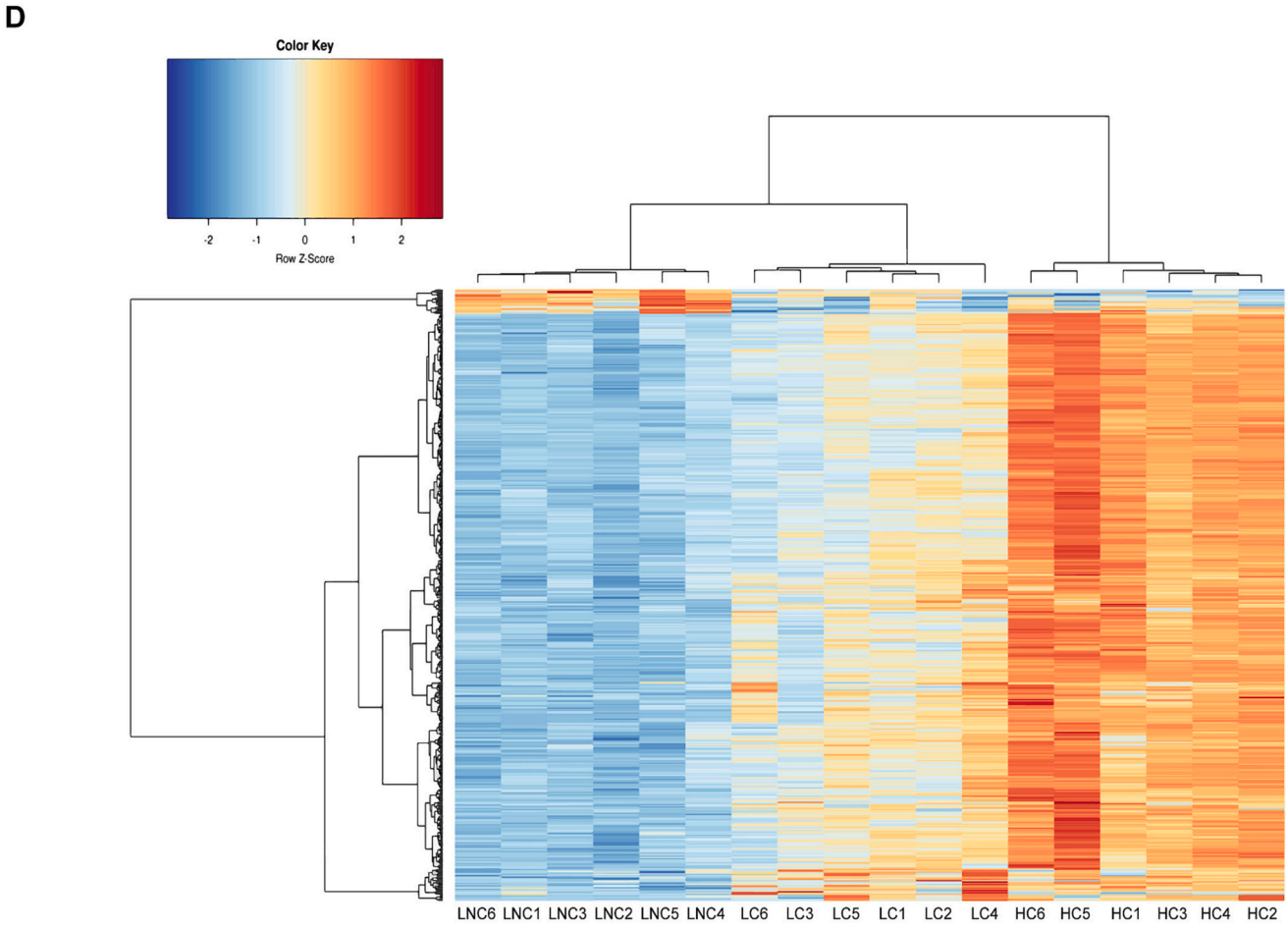

(caption on next page)

Fig. 3. RNA sequencing analysis of the cyst microenvironment. **(A)** Gene expression in LC and HC microdomains collected from the cyst microenvironment were compared to the distant LNC microdomains in the same kidneys. Differentially expressed genes (DEGs) per comparison were shown; HC vs LNC 8088 DEGs, LC vs LNC 953 DEGs, and HC vs LC 5929 DEGs. See Suppl. Table 3 for a complete list of DEGs. **(B)** Venn diagram showing the number of unique and shared DEGs between LC vs LNC, HC vs LNC, and HC vs LC comparisons. Please see Suppl. Table 4 for a list of unique and shared DEGs. **(C)** Volcano plots of the DEGs in the compared groups. All the genes were plotted and each data point represents a gene. The log2 fold change of each gene is represented on the x-axis and the log10 of its adjusted *p*-value is on the y-axis. Genes with an adjusted p-value <0.05 are indicated by red dots. **(D)** Heatmap of the top 500 DEGs in LC vs LNC comparison. Normalized expression of these genes were shown for all samples (6 microdomains per group (LNC, LC, or HC) collected from 3 male PKD mice with age 269 (2×) and 297 days).

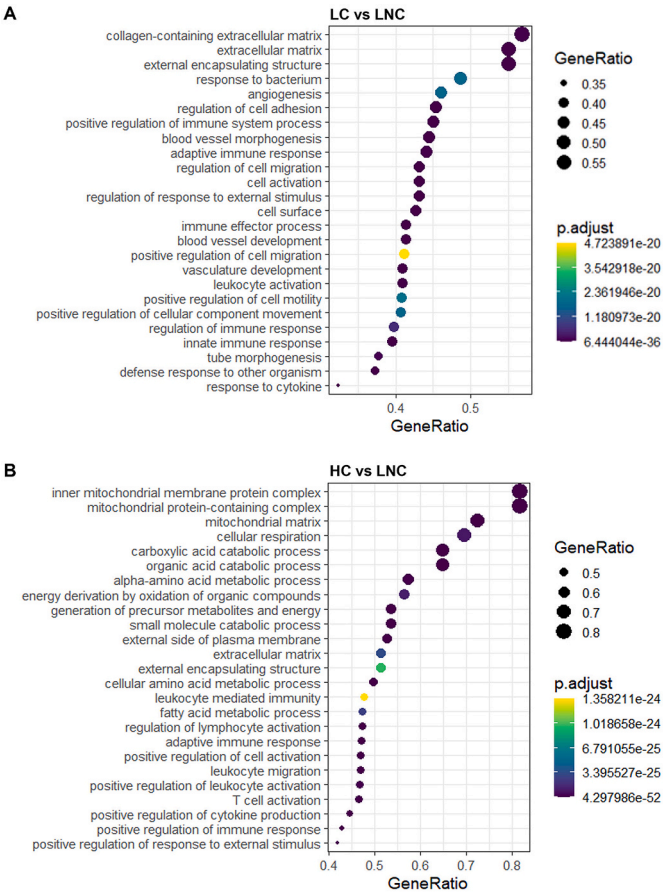

Fig. 4. Gene set enrichment analysis of the F4/80-low cyst microenvironment. Gene set enrichment analysis was performed using the gseGO() function and fold change ranked gene list using ClusterProfiler [91]. **(A** and **B)** Top 25 most significant enriched GO terms in LC (A) and HC (B) microdomains were ranked by GeneRatio and visualized using ggplot2. GeneRatio represents the ratio of number of enriched genes in the dataset associated with a GO term and the set size of that GO term. P.adjust represents adjusted p-value. See Suppl. Table 5 for a complete list of GO terms.

including NRF2-mediated Oxidative Stress Response pathway, which has been linked to ADPKD progression previously [54].

Collectively, these findings suggest that the tissue surrounding initial cysts already has activated injury-related signaling involving tissue remodeling, immune cell activation and mild metabolic dysfunction before macrophages accumulate in tissue. In macrophage-dense areas, these processes become more potentiated and are accompanied by the enrichment of several PKD-related signaling pathways and strongly altered metabolism. Dysregulated metabolic processes in HC microdomains compared to both LNC and LC microdomains suggests that these processes are more likely to be related to the immune cells.

3.7. Identification of early upstream regulators that may alter signaling in the cyst microenvironment

Since secreted factors are the most upstream molecules that can interact with their receptors and activate a certain signaling pathway in neighboring cells, we particularly focused on cytokines and growth factors using Upstream Regulator Analysis (URA) in IPA. We identified 22 cytokines and 9 growth factors that are predicted to have increased activity in LC microdomains based on differential expression of their target genes (Tables 1, 2, and Suppl. Table 7 ((complete list)). These cytokines were mainly inflammatory cytokines, including IFNγ, CSFs, interleukins, and TNF superfamily members (Table 1, URA panel). Among these cytokines, CSF1, IL33, and TNFSF13B also have significantly increased gene expression in LC microdomains compared to non-cystic regions, while for some other cytokines, the receptors were upregulated through which these cytokines exert their autocrine or paracrine signaling (e.g. IFNGR, TNFRSF1A, OSMR, TNFSRF12A, C5AR1, CSF2RA, and CD40) (Table 1, DGEA panels).

Among the predicted active growth factors, TGFB1, PDGFB, and FGF are multifunctional growth factors, that can promote cell growth, fibrosis, and EMT (Table 2, URA panel) [55–57]. Similarly, NRG1, AREG, and EGF are ligands of the ERBB family of receptor tyrosine kinases, which activate growth promoting pathways and regulate tissue regeneration [58]. Further, increased AGT/AGT-receptor activity could

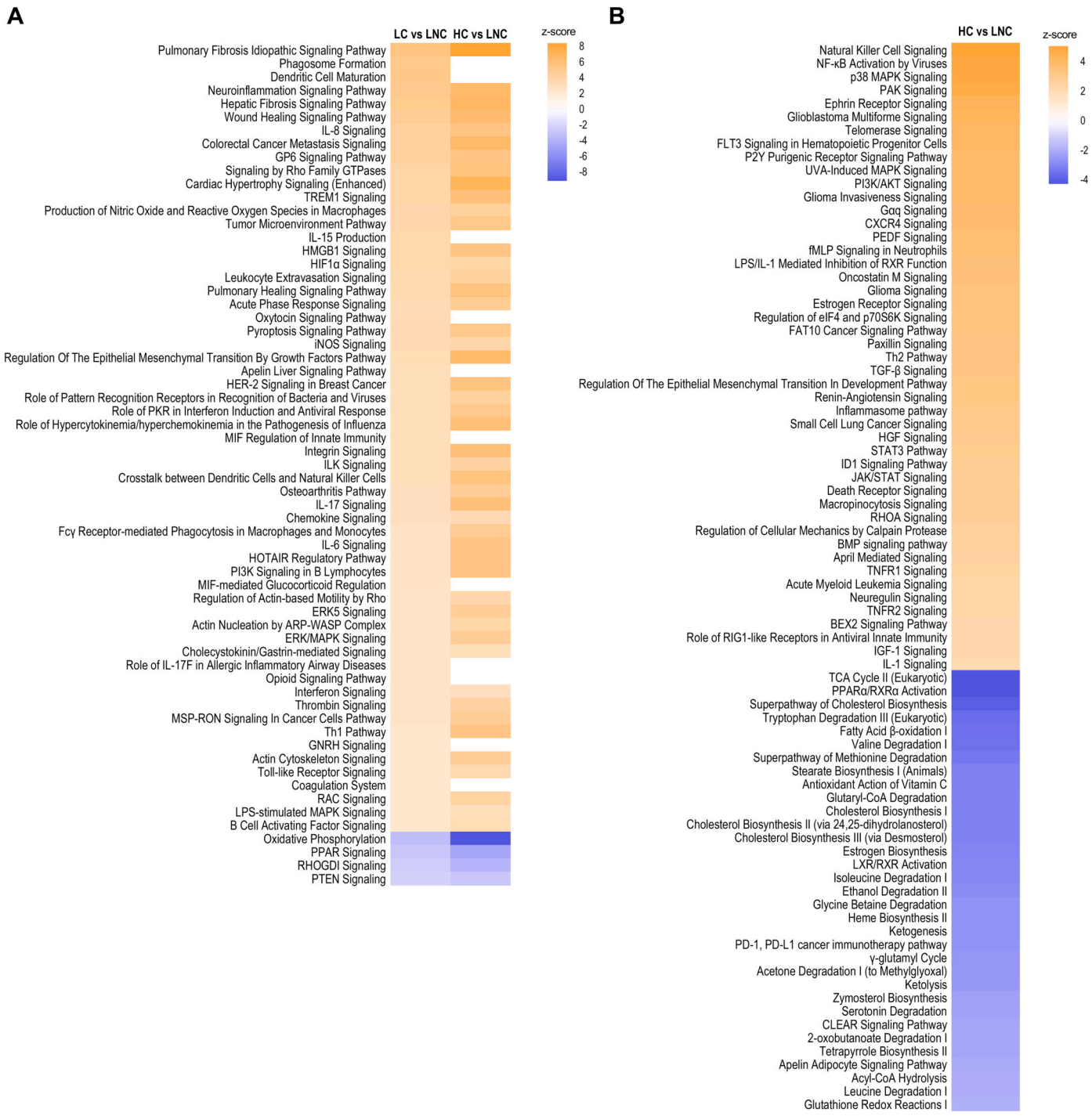

Fig. 5. Ingenuity pathway analysis of the cystic microenvironment. The heatmaps show significantly dysregulated canonical pathways with predicted significant activation (z-score > 2) in orange and significant inactivation (z-score < -2) in blue. Significant canonical pathways that were not predicted to be activated or inhibited were not shown in the figure. Please see Suppl. Table 6 for a complete overview of IPA. **(A)** Canonical pathways were ranked based on the z-score of the LC vs LNC comparison and include all significantly activated or inhibited canonical pathways for the LC vs LNC comparison. **(B)** Canonical pathways that were specifically activated or inhibited in HC microdomains compared to LNC.

directly be induced by mechanical stretch, promoting inflammatory, hypertrophic, and fibrotic responses [59–62]. In line with this, previous studies have shown improved kidney function, decreased cell proliferation, fibrosis, and inflammatory gene expression in PKD mice upon AGT mRNA suppression [45,63,64]. In addition to the increased predicted activity, gene expression of AGT and PDGFB was also increased, together with the TGFBR2 and PDGFRB expression (Table 2, DGEA panels). Together, these data suggest that several inflammatory cytokines and growth factors already have increased activity in macrophage-low regions near cysts, reflecting the secretory phenotype of injured tubular epithelial cells, which likely play a key role in epithelial cell proliferation, initiation of immune responses, and activation of tissue-repair/remodeling pathways in LC microdomains [61,65].

As expected, activity and expression of these cytokines and growth factors were increased in HC microdomains (higher z-score and fold

change), and additional cytokines and growth factors were identified that may contribute to the altered gene expression in HC microdomains (Suppl. Table 7 (complete list) and Suppl. Tables 8 and 9). Elevated expression and/or activity of secreted factors in HC microdomains is likely the result of increased release of these factors by accumulated immune cells, inflamed epithelial cells, and/or activated fibroblasts. Among these cytokines and growth factors, CCL2 (MCP-1), MIF, IGF1, TGFA, and CCN2 have been associated with ADPKD earlier [38,44,66–69]. These factors likely drive sustained activation of inflammatory and PKD-associated pathways in HC microdomains.

3.8. The effect of TWEAK and Oncostatin-M on cell proliferation and inflammatory response

It is well-known that the release of cytokines and growth factors recruits and activates immune cells and contributes to the regulation of injury responses [24]. Our upstream regulator analysis suggested several cytokines and growth factors as potential drivers of altered gene expression in the cyst microenvironment, including LC microdomains lacking immune cell infiltrates. Most of these factors were common pro-inflammatory cytokines (e.g. IFNG, TNF, and IL1B) and growth factors (e.g. TGFB1, AGT, and PDGFB), among which some have been studied in PKD as well [44,48,63,64,70]. To provide a proof-of-principle that these identified cytokines could also alter signaling in tubular epithelial cells and/or interstitial fibroblasts, in addition to their proposed effect on immune cells, we selected one known and one relatively unknown upstream regulator from the top 10 most active cytokines to evaluate their potential effect: TWEAK (TNFSF12, TNF-related weak inducer of apoptosis) and Oncostatin-M (OSM). The role of TWEAK in cystogenesis, cell proliferation, and inflammation has previously been studied in PKD mice, however, no in vitro experiments have been performed demonstrating a direct effect of TWEAK on epithelial cell proliferation [71]. Further, Oncostatin-M has not been linked to ADPKD pathogenesis previously, while it has been extensively studied in various types of cancer [72]. Therefore, TK173 (healthy human renal fibroblasts), *Pkd1*^{wt} and *Pkd1*$^{-/-}$ mouse proximal tubular epithelial cells (mPTECs) were stimulated with either TWEAK or Oncostatin-M. Both cytokines caused increased cell proliferation in TK173, *Pkd1*^{wt} and *Pkd1*$^{-/-}$ mPTECs (Fig. 6A-C). Also, a strong inflammatory response was induced in TK173, *Pkd1*^{wt} and *Pkd1*$^{-/-}$ mPTECs upon stimulation with TWEAK as assessed by increased *CSF1*, *IL6*, or *CCL2* gene expression after 24 h (Fig. 6D–F). Similarly, Oncostatin-M induced a robust *CSF1*, *IL6*, and *CCL2* expression in TK173 cells, while a subtle increase in *CCL2* expression was found in mPTECs (Fig. G–I). However, due to potential clonal variation that could be introduced during the generation of *Pkd1*$^{-/-}$ mPTECs, direct comparisons cannot be made between *Pkd1*^{wt} and *Pkd1*$^{-/-}$ cells, but both cell lines appear to respond to the stimuli. Collectively, our data show that the early upstream regulators TWEAK

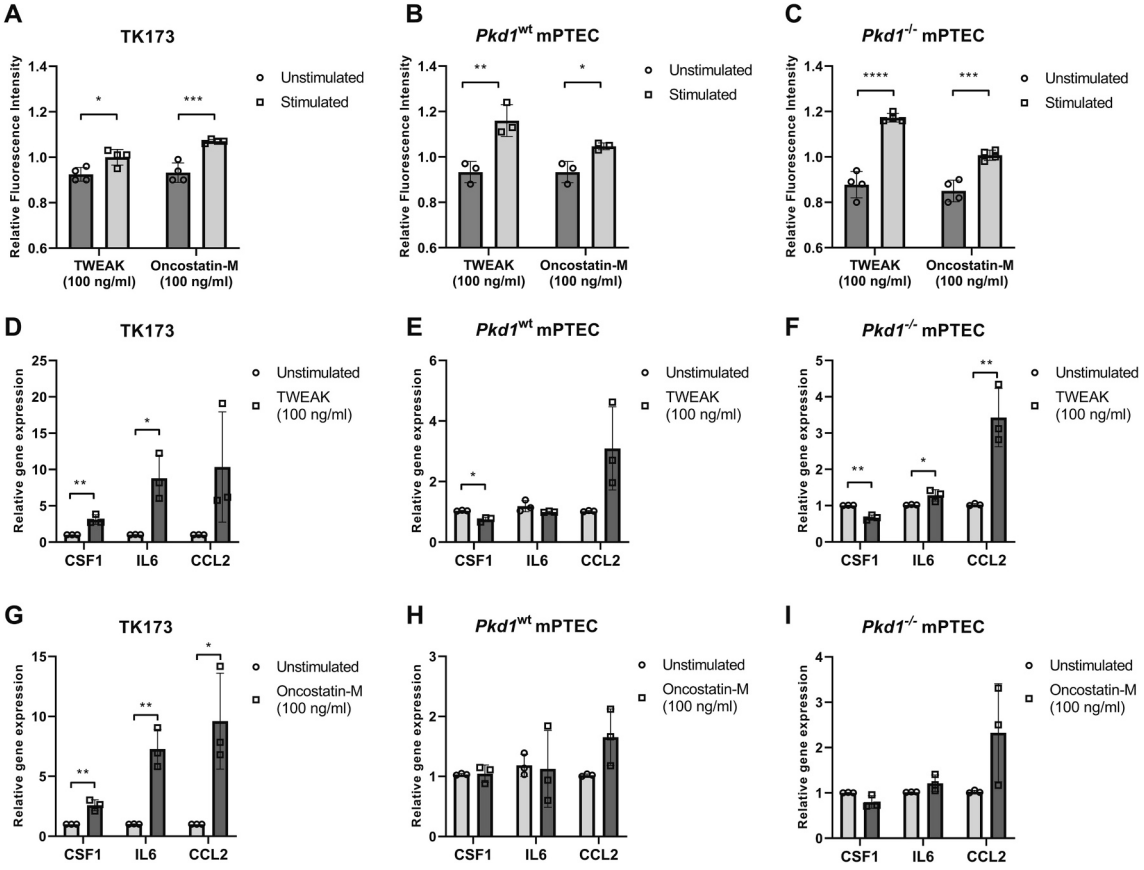

Fig. 6. The effect of TWEAK and Oncostatin-M on cell proliferation and inflammatory response in fibroblasts and epithelial cells in vitro. **(A–C)** TK173 cells (A), *Pkd1*^{wt} mPTECs (B), and *Pkd1*$^{-/-}$ mPTECs (C) were either unstimulated or stimulated with 100 ng/ml recombinant TWEAK or recombinant Oncostatin-M. After 24 h, cell proliferation was assessed using PrestoBlue reagent. 5 wells were treated per group per independent experiment and the average of 5 wells were shown as 1 data point in the graphs A–C. **(D–F)** TK173 cells (D), *Pkd1*^{wt} mPTECs (E), and *Pkd1*$^{-/-}$ mPTECs (F) were either unstimulated or stimulated with 100 ng/ml recombinant TWEAK. After 24 h, RNA was extracted from cells and gene expression of *CSF1*, *IL6*, and *CCL2* were analyzed using qPCR. **(G–I)** TK173 cells (G), *Pkd1*^{wt} mPTECs (H), and *Pkd1*$^{-/-}$ mPTECs (I) were either unstimulated or stimulated with 100 ng/ml recombinant Oncostatin-M. After 24 h, RNA was extracted from cells and gene expression of *CSF1*, *IL6*, and *CCL2* were analyzed using qPCR. (D–I) For qPCR experiments, 3 wells were treated per group per independent experiment, and the average of 3 wells were shown as 1 datapoint in the graphs. Data represent the mean ± SD. Significance was measured by unpaired *t*-test. * *P* value <0.05; ** P value <0.01; *** P value 0.001; **** P value 0.0001.

and Oncostatin-M promote cell proliferation and inflammatory gene expression in fibroblasts and both wild type and *Pkd1*-deficient tubular epithelial cells.

4. Discussion

By combining LCM and ultra-low input RNA sequencing, we have obtained a comprehensive overview of transcriptome alterations in the cyst microenvironment in iKsp-*Pkd1*^{del} mice. We compared gene expression profiles of both F4/80-low and F4/80-high cyst microenvironment with distant non-cystic regions and showed that the expression level of 953 and 8088 genes were altered, respectively. Our pathway analysis data indicates that the tissue surrounding initial cysts has activation of mechanical stress-, immune response-, fibrosis-, and cell growth-related pathways, and mild metabolic dysfunction before macrophages accumulate in tissue. Upon macrophage accumulation, these processes were more strongly dysregulated and were accompanied by alterations in various additional pathways, including various metabolic processes and ADPKD-related signaling pathways that have been reported previously [12,25,26,38,43–45,48–50,73,74]. In addition, we have investigated potential paracrine signaling-mediated alterations in the cyst microenvironment using upstream regulator analysis. By focusing on the secreted upstream molecules, we identified series of cytokines and growth factors that may drive early transcriptomic changes in F4/80-low cyst microenvironment and additional changes during inflammation in F4/80-high regions near cysts. Finally, we validated prioritized early upstream regulators TWEAK and Oncostatin-M and showed increased proliferation and inflammatory gene expression in epithelial cells and interstitial fibroblasts upon stimulation.

In the past decades, several studies have demonstrated that tissue resident macrophages could promote cyst growth and disease progression in PKD mouse models, leading to the identification of cytokines such as CSF1, MIF, and MCP1 as factors potentiating macrophage-dependent disease progression [66,67,71,75–77]. In the present study, we sought to profile alterations that occur in the cyst microenvironment that precede macrophage accumulation, which we referred to as the early alterations in the cyst microenvironment. For this purpose, F4/80-low regions near cysts were collected which also lacked T cells, B cells, and myofibroblasts. These regions also showed lower CD11b signal compared to F4/80-high microdomains, but we could not distinguish between resident and infiltrating macrophages by immunohistochemistry. Yet, these regions were characterized by activated injury-repair and tissue remodeling-related pathways. It is plausible that cyst expansion induces mechanical stress in the cyst microenvironment, leading to the activation of mechanical stress-related pathways such as Integrin Signaling, Signaling by Rho Family of GTPases, RAC Signaling, and Actin Cytoskeleton Signaling, which together regulate cellular responses to mechanical stress [40,41]. It is also possible that mechanical stretch near cysts induces epithelial cell injury, leading to the secretion of cytokines and growth factors that induce epithelial cell proliferation, activation of tissue repair and tissue remodeling-related pathways in LC microdomains. Therefore, we mainly focused on upstream cytokines and growth factors to examine which factors could induce paracrine-mediated altered signaling in the cyst microenvironment and identified: (1) series of cytokines and growth factors that may play an important role in epithelial cell-induced early injury-repair responses and cell proliferation in the cyst microenvironment before macrophage accumulation; (2) a wider variety of secreted factors in macrophage-dense regions that may contribute to sustained and uncontrolled inflammatory and profibrotic processes leading to maladaptive tissue repair, fibrosis and disease progression.

Among the identified early cytokines, we selected TWEAK and Oncostatin-M for validation, because of the increased activation score and increased expression of their receptors in LC microdomains. Both cytokines promoted cell proliferation and increased inflammatory gene expression in TK173 cells and mPTECs, suggesting that these cytokines not only target immune cells, but also affect interstitial fibroblasts and epithelial cells in the cyst microenvironment, likely causing a pro-proliferative and pro-inflammatory milieu before accumulation of macrophages and other immune cells. Thereby, these cytokines contribute to the dysregulation of signaling pathways in both *Pkd1*-deficient and wild type cells, and possibly also to the initiation of cyst formation and/or expansion. Previously, it was shown that TWEAK administration could induce and promote cystogenesis in *Pkd1*-dificient mice via activation of pro-proliferative pathways and the canonical NF-κB signaling, which could be restored with anti-TWEAK treatment [71]. Here we introduce Oncostatin-M as a novel potential candidate cytokine with a pro-proliferative and pro-inflammatory role in renal fibroblasts and renal epithelial cells.

Our data suggests that metabolic alterations mainly occur in HC microdomains and to a lesser extent in LC microdomains. It has been reported that regenerating epithelial cells could alter their metabolism, by switching from fatty acid oxidation (FAO) to glucose utilization, to adapt to the injury and to heal [61,78,79]. This may explain reduced oxidative phosphorylation and PPAR signaling in LC microdomains. Prolonged activation of cellular stress and injury-repair pathways in the cyst microenvironment probably cause accumulation of immune cells in the cyst microenvironment (HC microdomains), elevated levels of released cytokines and growth factors, enhanced injury-repair responses, tissue-remodeling, and sustained inflammation. In addition, increased secretion and activity of growth factors in HC microdomains (e.g. TGFB1 and CCN2) probably also result in the activation of fibroblasts, which in turn promote fibrosis and cystic epithelial cell proliferation [80,81].

Reduced FAO in tubular epithelial cells has also been associated with ATP depletion, cell death, epithelial cell dedifferentiation and lipid accumulation previously [82]. Also, excess of fatty acids have been reported to alter mitochondrial function, enhance tubular inflammation and promote endoplasmic reticulum stress, contributing to epithelial injury, fibrosis, and inflammation [83]. It is also possible that the metabolic switch that occurs in injured cells in order to allow tissue repair, causes excess fatty acid accumulation in and around cells during prolonged injury in the cyst microenvironment, inducing more metabolic defects in epithelial cells, inflammation and fibrosis. However, epithelial cells in the cyst microenvironment could also switch to glycolysis because of mitochondrial defects caused by the lack of PC1, or due to increased ROS production caused by chronic inflammation [84–86]. Further, increased metabolic alterations in HC microdomains may be a reflection of macrophage accumulation as well, since activated macrophages also show increased aerobic glycolysis and other metabolic changes dependent on the stimuli and their polarization [87]. Therefore, increased metabolic alterations in HC microdomains are likely (partially) a reflection of macrophage accumulation.

Furthermore, pathways frequently associated with ADPKD progression were mainly dysregulated in HC microdomains, including activated p70S6K, PI3K/AKT, CXCR4, TGF-β, Renin-Angiotensin, HGF, STAT3, JAK/STAT, TNFR, IGF-1 signaling, and reduced Oxidative Phosphorylation, Fatty Acid β-oxidation, PPARa/RXRa activation, and TCA cycle [25,38,42–48,50,74,88–90]. These data suggest that many processes associated with advanced PKD are primarily concentrated in macrophage- and myofibroblast-dense cyst microenvironment, although lower levels of activity might still occur in the LC microdomains.

The use of microdomains rather than single cells has limited our understanding of altered signaling in different cell types in the cyst microenvironment. Therefore, it remains to be elucidated which cells have altered metabolism, which cells secrete and respond to the identified secreted factors and how different cell types interact in the cyst microenvironment and contribute to the cystic snowball effect. However, the use of microdomains has the advantage that it contains spatial information which would be lost with single cell sequencing. So far, this is the first comprehensive analysis of the cyst microenvironment in PKD to unravel altered transcriptome, while preserving the spatial context of the tissue.

Collectively, it is clear that the cyst microenvironment has a highly altered transcriptome when compared to the non-cystic parts in the same kidney, even before the infiltration of macrophages. Macrophage accumulation seems to occur upon a wide variety of transcriptomic changes in the cyst microenvironment, such as altered metabolism, activation of injury-repair pathways and tissue remodeling. Sustained mechanical stress, unresolved injury, and prolonged secretion of various cytokines and growth factors potentially lead to immune cell and myofibroblast accumulation in designated areas in the cyst microenvironment, leading to the dysregulation of wider variety of pathways. Our upstream regulator analysis identifies and prioritizes paracrine factors that may drive early alterations in the cyst microenvironment and potentially give rise to the formation of more cysts.

Supplementary data to this article can be found online at https://doi.org/10.1016/j.bbadis.2023.166987.

Funding

This study was supported by the Dutch Kidney Foundation (grant 19OP012).

CRediT authorship contribution statement

Sevtap A. Yasinoglu: Conceptualization, Data curation, Formal analysis, Investigation, Methodology, Project administration, Visualization, Writing – original draft, Writing – review & editing. **Thomas B. Kuipers:** Data curation, Formal analysis, Software, Visualization. **Ernst Suidgeest:** Investigation, Visualization. **Louise van der Weerd:** Conceptualization, Methodology, Supervision. **Hailiang Mei:** Conceptualization, Methodology, Supervision. **Hans J. Baelde:** Conceptualization, Data curation, Methodology, Project administration, Resources, Supervision, Writing – review & editing. **Dorien J.M. Peters:** Conceptualization, Data curation, Funding acquisition, Methodology, Project administration, Resources, Supervision, Writing – review & editing.

Declaration of competing interest

The authors declare the following financial interests/personal relationships which may be considered as potential competing interests:

D.J.M. Peters reports financial support was provided by Dutch Kidney Foundation. D.J.M. Peters reports a relationship with Mironid Ltd. that includes: consulting or advisory. D.J.M. Peters reports a relationship with Crown Bioscience Inc. that includes: consulting or advisory. D.J.M. Peters reports a relationship with Innoser Laboratories BV that includes: consulting or advisory.

Data availability

RNA sequencing datasets generated during this study are available in the Gene Expression Omnibus repository (GEO, http://www.ncbi.nlm.nih.gov/geo/, accession number: GSE231304).

Acknowledgments

We would like to gratefully thank Kyra Dijkstra, Emile Meijer, and Oleh DzyuBachyk for their technical assistance, and Susan Kloet and Kees Fluiter for advice.

References

[1] C.J. Willey, et al., Prevalence of autosomal dominant polycystic kidney disease in the European Union, Nephrology Dialysis Transplantation 32 (8) (2017) 1356–1363.
[2] T.T. Aung, et al., Autosomal dominant polycystic kidney disease prevalence among a racially diverse United States population, 2002 through 2018, Kidney 360 (2021) 2010–2015, 2(12).
[3] T. Mochizuki, et al., PKD2, a gene for polycystic kidney disease that encodes an integral membrane protein, Science 272 (5266) (1996) 1339–1342.
[4] C.J. Ward, et al., The polycystic kidney-disease-1 gene encodes a 14-kb transcript and lies within a duplicated region on chromosome-16, Cell 77 (6) (1994) 881–894.
[5] P.C. Harris, V.E. Torres, in: M.P. Adam, et al. (Eds.), Polycystic Kidney Disease, Autosomal Dominant, GeneReviews(®), University of Washington, 1993. Seattle Copyright © 1993-2022, University of Washington, Seattle. GeneReviews is a registered trademark of the University of Washington, Seattle. All rights reserved.: Seattle (WA).
[6] P.S. Shen, et al., The structure of the polycystic kidney disease channel PKD2 in lipid nanodiscs, Cell 167 (3) (2016) 763–773.e11.
[7] M. Grieben, et al., Structure of the polycystic kidney disease TRP channel polycystin-2 (PC2), Nat. Struct. Mol. Biol. 24 (2) (2017) 114–122.
[8] M. Wilkes, et al., Molecular insights into lipid-assisted Ca(2+) regulation of the TRP channel polycystin-2, Nat. Struct. Mol. Biol. 24 (2) (2017) 123–130.
[9] Z. Wang, et al., The ion channel function of polycystin-1 in the polycystin-1/polycystin-2 complex, EMBO Rep. 20 (11) (2019), e48336.
[10] C. Bergmann, et al., Polycystic kidney disease, Nat. Rev. Dis. Primers. (2018) 4.
[11] I. Rowe, et al., Defective glucose metabolism in polycystic kidney disease identifies a new therapeutic strategy, Nat. Med. 19 (4) (2013) 488–493.
[12] L.F. Menezes, et al., Fatty acid oxidation is impaired in an orthologous mouse model of autosomal dominant polycystic kidney disease, Ebiomedicine 5 (2016) 183–192.
[13] P.S. Parfrey, et al., The diagnosis and prognosis of autosomal dominant polycystic kidney-disease, N. Engl. J. Med. 323 (16) (1990) 1085–1090.
[14] S. Lavu, et al., *The value of genotypic and imaging information to predict functional and structural outcomes in ADPKD.* JCI, Insight 5 (15) (2020).
[15] V.E. Torres, et al., Multicenter study of long-term safety of tolvaptan in later-stage autosomal dominant polycystic kidney disease, Clin. J. Am. Soc. Nephrol. 16 (1) (2021) 48–58.
[16] F. Qian, et al., The molecular basis of focal cyst formation in human autosomal dominant polycystic kidney disease type I, Cell 87 (6) (1996) 979–987.
[17] S.T. Reeders, Multilocus polycystic disease, Nat. Genet. 1 (4) (1992) 235–237.
[18] S.T. Jiang, et al., Defining a link with autosomal-dominant polycystic kidney disease in mice with congenitally low expression of Pkd1, Am. J. Pathol. 168 (1) (2006) 205–220.
[19] Y. Pei, A "two-hit" model of cystogenesis in autosomal dominant polycystic kidney disease? Trends Mol. Med. 7 (4) (2001) 151–156.
[20] I.S. Lantinga-van Leeuwen, et al., Lowering of Pkd1 expression is sufficient to cause polycystic kidney disease, Hum. Mol. Genet. 13 (24) (2004) 3069–3077.
[21] K. Hopp, et al., Functional polycystin-1 dosage governs autosomal dominant polycystic kidney disease severity, J. Clin. Investig. 122 (11) (2012) 4257–4273.
[22] W.N. Leonhard, et al., Scattered deletion of PKD1 in kidneys causes a cystic snowball effect and recapitulates polycystic kidney disease, J. Am. Soc. Nephrol. 26 (6) (2015) 1322–1333.
[23] W.N. Leonhard, H. Happe, D.J.M. Peters, Variable cyst development in autosomal dominant polycystic kidney disease: the biologic context, J. Am. Soc. Nephrol. 27 (12) (2016) 3530–3538.
[24] C. Formica, D.J.M. Peters, Molecular pathways involved in injury-repair and ADPKD progression, Cell. Signal. 72 (2020).
[25] T.B. Malas, et al., Meta-analysis of polycystic kidney disease expression profiles defines strong involvement of injury repair processes (vol 312, pg F806-F817, 2017), American Journal of Physiology-Renal Physiology 314 (1) (2018) F140.
[26] T.B. Malas, et al., Prioritization of novel ADPKD drug candidates from disease-stage specific gene expression profiles, Ebiomedicine (2020) 51.
[27] L.F. Menezes, G.G. Germino, Systems biology of polycystic kidney disease: a critical review, Wiley Interdisciplinary Reviews-Systems Biology and Medicine 7 (1) (2015) 39–52.
[28] Z. Li, K.A. Zimmerman, B.K. Yoder, Resident macrophages in cystic kidney disease, Kidney360 2 (1) (2021) 167.
[29] I.S. Lantinga-van Leeuwen, et al., Kidney-specific inactivation of the Pkd1 gene induces rapid cyst formation in developing kidneys and a slow onset of disease in adult mice, Hum. Mol. Genet. 16 (24) (2007) 3188–3196.
[30] E.M. Glare, et al., beta-Actin and GAPDH housekeeping gene expression in asthmatic airways is variable and not suitable for normalising mRNA levels, Thorax 57 (9) (2002) 765–770.
[31] T. Montero-Melendez, M. Perretti, Gapdh gene expression is modulated by inflammatory arthritis and is not suitable for qPCR normalization, Inflammation 37 (4) (2014) 1059–1069.
[32] J.J. Muñoz, et al., Ppia is the most stable housekeeping gene for qRT-PCR normalization in kidneys of three Pkd1-deficient mouse models, Sci. Rep. 11 (1) (2021) 19798.
[33] S. Picelli, et al., Smart-seq2 for sensitive full-length transcriptome profiling in single cells, Nat. Methods 10 (11) (2013) 1096–1098.
[34] A. Krämer, et al., Causal analysis approaches in ingenuity pathway analysis, Bioinformatics 30 (4) (2014) 523–530.
[35] F. Petitprez, et al., The murine microenvironment cell population counter method to estimate abundance of tissue-infiltrating immune and stromal cell populations in murine samples using gene expression, Genome Med. 12 (1) (2020) 86.
[36] W.N. Leonhard, et al., Curcumin inhibits cystogenesis by simultaneous interference of multiple signaling pathways: in vivo evidence from a Pkd1-deletion model, Am. J. Physiol. Renal Physiol. 300 (5) (2011) F1193–F1202.
[37] G.A. Müller, et al., Human renal fibroblast cell lines (tFKIF and tNKF) are new tools to investigate pathophysiologic mechanisms of renal interstitial fibrosis, Exp. Nephrol. 3 (2) (1995) 127–133.

[38] S. Kashyap, et al., *Metalloproteinase PAPP−a regulation of IGF−1 contributes to polycystic kidney disease pathogenesis.* Jci, Insight 5 (4) (2020).
[39] J.A.M.J.L. Janssen, New insights from IGF-IR stimulating activity analyses: pathological considerations, Cells 9 (4) (2020).
[40] J.L. Hoon, M.H. Tan, C.G. Koh, The regulation of cellular responses to mechanical cues by rho GTPases, Cells 5 (2) (2016).
[41] C. Ruwhof, A. van der Laarse, Mechanical stress-induced cardiac hypertrophy: mechanisms and signal transduction pathways, Cardiovasc. Res. 47 (1) (2000) 23–37.
[42] G. Distefano, et al., Polycystin-1 regulates extracellular signal-regulated kinase-dependent phosphorylation of tuberin to control cell size through mTOR and its downstream effectors S6K and 4EBP1, Mol. Cell. Biol. 29 (9) (2009) 2359–2371.
[43] H. Kim, et al., Expression and secretion of CXCL12 are enhanced in autosomal dominant polycystic kidney disease, BMB Rep. 52 (7) (2019) 463–468.
[44] S. Hassane, et al., Elevated TGFbeta-Smad signalling in experimental Pkd1 models and human patients with polycystic kidney disease, J. Pathol. 222 (1) (2010) 21–31.
[45] T. Saigusa, et al., Activation of the intrarenal renin-angiotensin-system in murine polycystic kidney disease, Physiol. Rep. 3 (5) (2015).
[46] S. Qin, et al., Failure to ubiquitinate c-Met leads to hyperactivation of mTOR signaling in a mouse model of autosomal dominant polycystic kidney disease, J. Clin. Invest. 120 (10) (2010) 3617–3628.
[47] A. Viau, et al., Tubular STAT3 limits renal inflammation in autosomal dominant polycystic kidney disease, J. Am. Soc. Nephrol. 31 (5) (2020) 1035–1049.
[48] J.X. Zhou, et al., TNFα signaling regulates cystic epithelial cell proliferation through Akt/mTOR and ERK/MAPK/Cdk2 mediated Id2 signaling, PloS One 10 (6) (2015), e0131043.
[49] C. Xu, et al., Attenuated, flow-induced ATP release contributes to absence of flow-sensitive, purinergic Cai2+ signaling in human ADPKD cyst epithelial cells, Am. J. Physiol. Renal Physiol. 296 (6) (2009) F1464–F1476.
[50] Z. Novalic, et al., Dose-dependent effects of sirolimus on mTOR signaling and polycystic kidney disease, J. Am. Soc. Nephrol. 23 (5) (2012) 842–853.
[51] A. Aichem, M. Groettrup, The ubiquitin-like modifier FAT10 in cancer development, Int. J. Biochem. Cell Biol. 79 (2016) 451–461.
[52] S. Ghareghomi, et al., Fundamental insights into the interaction between telomerase/TERT and intracellular signaling pathways, Biochimie 181 (2021) 12–24.
[53] C.K. Rane, A. Minden, P21 activated kinase signaling in cancer, Semin. Cancer Biol. 54 (2019) 40–49.
[54] Y. Lu, et al., Activation of NRF2 ameliorates oxidative stress and cystogenesis in autosomal dominant polycystic kidney disease, Sci. Transl. Med. 12 (554) (2020) p. eaba3613.
[55] Y. Xie, et al., FGF/FGFR signaling in health and disease, Signal Transduct. Target. Ther. 5 (1) (2020) 181.
[56] X. Zou, et al., Targeting the PDGF/PDGFR signaling pathway for cancer therapy: a review, Int. J. Biol. Macromol. 202 (2022) 539–557.
[57] M. Morikawa, R. Derynck, K. Miyazono, TGF-β and the TGF-β Family: Context-Dependent Roles in Cell and Tissue Physiology 8(5), Cold Spring Harb Perspect Biol, 2016.
[58] M.I. Parker, et al., Proliferative signaling by ERBB proteins and RAF/MEK/ERK effectors in polycystic kidney disease, Cell. Signal. 67 (2020), 109497.
[59] G. Liu, et al., Mechanical stretch potentiates angiotensin II-induced proliferation in spontaneously hypertensive rat vascular smooth muscle cells, Hypertens. Res. 33 (12) (2010) 1250–1257.
[60] L. Hunyady, G. Turu, The role of the AT1 angiotensin receptor in cardiac hypertrophy: angiotensin II receptor or stretch sensor? Trends in Endocrinology & Metabolism 15 (9) (2004) 405–408.
[61] B.C. Liu, et al., Renal tubule injury: a driving force toward chronic kidney disease, Kidney Int. 93 (3) (2018) 568–579.
[62] N. Yasuda, et al., A novel mechanism of mechanical stress-induced angiotensin II type 1–receptor activation without the involvement of angiotensin II, Naunyn Schmiedebergs Arch. Pharmacol. 377 (4) (2008) 393–399.
[63] K. Ravichandran, et al., Antisense-mediated angiotensinogen inhibition slows polycystic kidney disease in mice with a targeted mutation in Pkd2, Am. J. Physiol. Renal Physiol. 308 (4) (2015) F349–F357.
[64] T. Saigusa, et al., Suppressing angiotensinogen synthesis attenuates kidney cyst formation in a Pkd1 mouse model, FASEB J. 30 (1) (2016) 370–379.
[65] D. Zhou, Y.H. Liu, RENAL FIBROSIS IN 2015 understanding the mechanisms of kidney fibrosis, Nat. Rev. Nephrol. 12 (2) (2016) 68–70.
[66] M.F. Cassini, et al., Mcp1 promotes macrophage-dependent cyst expansion in autosomal dominant polycystic kidney disease, J. Am. Soc. Nephrol. 29 (10) (2018) 2471–2481.
[67] L. Chen, et al., Macrophage migration inhibitory factor promotes cyst growth in polycystic kidney disease, J. Clin. Investig. 125 (6) (2015) 2399–2412.
[68] N. Dwivedi, et al., Epithelial vasopressin type-2 receptors regulate myofibroblasts by a YAP-CCN2-dependent mechanism in polycystic kidney disease, J. Am. Soc. Nephrol. 31 (8) (2020) 1697–1710.
[69] D.C.W. Lee, K.W. Chan, S.Y. Chan, Expression of transforming growth factor alpha and epidermal growth factor receptor in adult polycystic kidney disease, J. Urol. 159 (1) (1998) 291–296.
[70] P.D. Wilson, J. Du, J.T. Norman, Autocrine, endocrine and paracrine regulation of growth abnormalities in autosomal-dominant polycystic kidney-disease, Eur. J. Cell Biol. 61 (1) (1993) 131–138.
[71] A. Cordido, et al., TWEAK signaling pathway blockade slows cyst growth and disease progression in autosomal dominant polycystic kidney disease, J. Am. Soc. Nephrol. 32 (8) (2021) 1913–1932.
[72] A. Masjedi, et al., Oncostatin M: a mysterious cytokine in cancers, Int. Immunopharmacol. 90 (2021), 107158.
[73] J.M. Shillingford, et al., Rapamycin ameliorates PKD resulting from conditional inactivation of Pkd1, J. Am. Soc. Nephrol. 21 (3) (2010) 489–497.
[74] J.J. Talbot, et al., Polycystin-1 regulates STAT activity by a dual mechanism, Proc. Natl. Acad. Sci. U. S. A. 108 (19) (2011) 7985–7990.
[75] A. Karihaloo, et al., Macrophages promote cyst growth in polycystic kidney disease, J. Am. Soc. Nephrol. 22 (10) (2011) 1809–1814.
[76] K.I. Swenson-Fields, et al., Macrophages promote polycystic kidney disease progression, Kidney Int. 83 (5) (2013) 855–864.
[77] K.A. Zimmerman, et al., Tissue-resident macrophages promote renal cystic disease, J. Am. Soc. Nephrol. 30 (10) (2019) 1841–1856.
[78] R.P. Lan, et al., Mitochondrial pathology and glycolytic shift during proximal tubule atrophy after ischemic AKI, J. Am. Soc. Nephrol. 27 (11) (2016) 3356–3367.
[79] Z.Z. Li, S. Lu, X.B. Li, The role of metabolic reprogramming in tubular epithelial cells during the progression of acute kidney injury, Cell. Mol. Life Sci. 78 (15) (2021) 5731–5741.
[80] N. Dwivedi, et al., Epithelial vasopressin type-2 receptors regulate myofibroblasts by a YAP-CCN2–dependent mechanism in polycystic kidney disease, J. Am. Soc. Nephrol. 31 (8) (2020).
[81] N. Dwivedi, et al., Myofibroblast depletion reduces kidney cyst growth and fibrosis in autosomal dominant polycystic kidney disease, Kidney Int. 103 (1) (2023) 144–155.
[82] H.M. Kang, et al., Defective fatty acid oxidation in renal tubular epithelial cells has a key role in kidney fibrosis development, Nat. Med. 21 (1) (2015) 37–46.
[83] N. Simon, A. Hertig, Alteration of fatty acid oxidation in tubular epithelial cells: from acute kidney injury to renal fibrogenesis, Front. Med. (2015) 2.
[84] X.Y. Liu, et al., Role of abnormal energy metabolism in the progression of chronic kidney disease and drug intervention, Ren. Fail. 44 (1) (2022) 790–805.
[85] H.R. Griffiths, D. Gao, C. Pararasa, Redox regulation in metabolic programming and inflammation, Redox Biol. 12 (2017) 50–57.
[86] V. Padovano, et al., The polycystins are modulated by cellular oxygen sensing pathways and regulate mitochondrial function, Mol. Biol. Cell 28 (2017).
[87] S.Y. Wang, et al., Metabolic reprogramming of macrophages during infections and cancer, Cancer Lett. 452 (2019) 14–22.
[88] J.P. Margaria, et al., The PI3K/Akt/mTOR pathway in polycystic kidney disease: a complex interaction with polycystins and primary cilium, Cell. Signal. 66 (2020), 109468.
[89] Y. Zhang, et al., Overexpression of TGF-beta1 induces renal fibrosis and accelerates the decline in kidney function in polycystic kidney disease, Am. J. Physiol. Renal Physiol. 319 (6) (2020) F1135–F1148.
[90] C. Podrini, L. Cassina, A. Boletta, Metabolic reprogramming and the role of mitochondria in polycystic kidney disease, Cell. Signal. 67 (2020), 109495.
[91] T.Z. Wu, et al., clusterProfiler 4.0: a universal enrichment tool for interpreting omics data, Innovation 2 (3) (2021).